

The Link between the Baryonic Mass Distribution and the Rotation Curve Shape

R. A. Swaters,¹ * R. Sancisi,^{2,3} J. M. van der Hulst,³ T. S. van Albada³

¹ National Optical Astronomy Observatory, 950 North Cherry Ave., Tucson, AZ 85719

² INAF - Osservatorio Astronomico di Bologna, via Ranzani 1, 40127 Bologna, Italy

³ Kapteyn Astronomical Institute, University of Groningen, Landleven 12, 9747 AD Groningen, the Netherlands

2 June 2021

ABSTRACT

The observed rotation curves of disc galaxies, ranging from late-type dwarf galaxies to early-type spirals, can be fit remarkably well simply by scaling up the contributions of the stellar and H I discs. This ‘baryonic scaling model’ can explain the full breadth of observed rotation curves with only two free parameters. For a small fraction of galaxies, in particular early-type spiral galaxies, HI scaling appears to fail in the outer parts, possibly due to observational effects or ionization of the H I. The overall success of the baryonic scaling model suggests that the well-known global coupling between the baryonic mass of a galaxy and its rotation velocity (known as the baryonic Tully-Fisher relation), applies at a more local level as well, and it seems to imply a link between the baryonic mass distribution and the distribution of total mass (including dark matter).

Key words: galaxies: dwarf – galaxies: kinematics and dynamics – Galaxies: spiral.

1 INTRODUCTION

Over the bright optical part of spiral galaxy discs, observed rotation curves can usually be explained by the contribution of the stars alone (e.g., Kalnajs 1983; Kent 1986). In this so-called maximum disc hypothesis, the contribution of stellar disc to the rotation curve is maximized, and that of the dark matter is minimized (e.g., van Albada et al. 1985; Begeman 1987; Broeils 1992a). However, even though the contribution of the stellar disc can be scaled to explain the inner rotation curve, good fits can usually be obtained for a range of contributions of the stellar discs, including submaximal and minimal discs (e.g., van Albada et al. 1985; Verheijen 1997; Swaters 1999; Dutton et al. 2005; Noordermeer 2006).

In almost all galaxies the contribution of the stellar disc can be scaled to explain all of the observed rotation curve out to about two or three disc scale lengths (e.g., Kalnajs 1983; Kent 1986; Palunas & Williams 2000), regardless of the relative contribution of the stellar disc to the rotation curve. This is not an argument that discs are maximal, but it does indicate that the total mass density (which includes the dark matter) and the luminous mass density are closely coupled (e.g., Sancisi 2004; Swaters et al. 2009).

This link between the distributions of luminous mass and total mass is not limited to spiral galaxies. Recently, Swaters et al. (2011) showed that for all but one of the late-type dwarf galaxies in their sample, the contribution of the stellar disc to the rotation curve can also be scaled up to explain most of the inner parts of the observed

rotation curves. Even though these galaxies may not actually have maximal discs, because the required stellar mass-to-light ratios are high, up to about 15 in the R -band, the fact that the stellar disc can be scaled to explain the inner two or three disc scale lengths of the rotation curves demonstrates that the apparent coupling between luminous and total mass density extends to late-type dwarf galaxies as well.

Interestingly, the apparent coupling between the rotation curve shape and the visible matter works not only for the stellar disc, but also for the H I disc. Bosma (1978, 1981) found that the ratio of total mass surface density to H I surface density is roughly constant in the outer parts of galaxies. He also found that the ratio decreased towards galaxies with lower rotation velocities. This proportionality of H I to dark mass surface density was later found in late-type dwarf galaxies (Carignan 1985; Carignan & Puche 1990; Jobin & Carignan 1990).

Hoekstra, van Albada & Sancisi (2001; hereafter HvAS) tested the hypothesis that the H I disc can be scaled up to explain the outer rotation curve for the large sample of galaxies presented in Broeils (1992a), which spans a large range in galaxy properties. HvAS found that for most of the galaxies in this sample the rotation curves can be explained well by scaling up the H I contribution by a factor of around 10, in combination with a maximal optical disc. In contrast with Bosma (1978), HvAS found that the H I scaling factor was independent of the maximum rotation velocity. They noted that among early-type spiral galaxies H I scaling was less successful at explaining the observed rotation curves. They did not conclude that there is a real coupling between HI and dark matter.

* E-mail: rob@swaters.net

Table 1. Optical and dark matter properties

UGC (1)	Source (2)	T (3)	D_a (4)	M_R (5)	h (6)	μ_0^R (7)	r_{imp}/h (8)	v_{imp} (9)	i (10)	$\Upsilon_{\text{d,MD}}^R$ (11)	χ_{MD}^2 (12)	$\Upsilon_{\text{d,HI}}^R$ (13)	η (14)	χ_{HI}^2 (15)
731	dwarf	10	8.0	-16.6	1.7	23.0	4.2	74	57	15.1	0.5	14.0 ± 1.2	3.8 ± 0.8	0.2
2916	early	2	63.5	-22.0	5.0	21.0	7.4	181	42	5.2	0.4	4.9 ± 1.0	5.2 ± 1.4	0.5
2953	early	2	15.1	-22.5	4.1	19.3	14.6	283	50	5.4	2.0	5.1 ± 0.2	45 ± 3	3.0
3205	early	2	48.7	-21.9	3.5	19.6	11.1	219	67	4.5	4.0	4.5 ± 0.2	10.6 ± 0.6	5.4
3371	dwarf	10	12.8	-17.7	3.1	23.3	3.3	86	49	12.5	0.7	12.1 ± 1.0	4.9 ± 1.0	0.5
3546	early	1	27.3	-21.4	2.8	19.5	10.0	193	55	4.0	1.0	4.6 ± 0.3	20 ± 3	1.4
3580	early	1	19.2	-19.4	2.4	21.6	10.5	124	63	7.2	3.2	5.1 ± 0.5	10.9 ± 0.6	3.4
4325	dwarf	9	10.1	-18.1	1.6	21.6	3.6	92	41	9.1	1.8	8.9 ± 0.8	0.8 ± 0.8	1.1
4499	dwarf	8	13.0	-17.8	1.5	21.5	5.7	74	50	2.3	0.6	3.1 ± 0.5	5.3 ± 0.5	1.0
5414	dwarf	10	10.0	-17.6	1.5	21.8	2.9	61	55	4.6	1.1	3.1 ± 0.9	3.9 ± 1.6	0.8
6399	UMa	9	18.6	-18.7	2.2	22.2	3.7	88	75	2.7	0.1	2.9 ± 0.6	6.4 ± 2.5	0.1
6446	dwarf	7	12.0	-18.4	1.9	21.4	5.1	80	52	4.0	0.4	4.3 ± 0.3	5.0 ± 0.5	1.1
6446	UMa	7	18.6	-18.9	3.1	22.2	5.1	80	51	3.2	0.7	3.0 ± 0.2	3.2 ± 0.5	0.8
6537	UMa	5	18.6	-21.7	5.2	20.1	6.5	167	53	1.7	2.3	1.7 ± 0.1	5.3 ± 0.9	10.1
6595	UMa	3	18.6	-20.4	1.8	19.5	21.0	113	76	0.8	0.8	0.5 ± 0.2	12.9 ± 1.3	0.8
6745	UMa	5	18.6	-21.6	3.0	19.1	3.9	169	76	0.6	1.3	1.8 ± 0.2	4.7 ± 3.4	2.0
6778	UMa	5	18.6	-18.7	2.5	19.3	8.4	148	49	1.7	1.4	1.6 ± 0.2	10.9 ± 1.6	3.0
6786	early	-1	25.9	-21.1	1.5	19.3	20.1	211	68	3.6	1.7	7.6 ± 0.7	42 ± 3	4.8
6787	early	2	18.9	-32.3	3.3	20.5	10.1	255	69	9.3	3.4	8.1 ± 0.2	52 ± 4	2.6
6815	UMa	6	18.6	-20.8	2.9	20.9	5.3	137	79	1.6	2.0	2.3 ± 0.1	7.4 ± 1.3	2.8
6869	UMa	4	18.6	-21.0	1.7	19.2	4.3	169	55	0.5	1.0	1.1 ± 0.1	10.1 ± 2.6	2.5
6870	UMa	4	18.6	-22.1	3.9	19.5	4.2	215	62	2.3	0.6	2.6 ± 0.1	11.1 ± 3.0	1.0
6904	UMa	4	18.6	-20.2	2.1	19.9	4.4	134	77	1.5	0.9	1.8 ± 0.2	12.6 ± 2.3	1.2
6917	UMa	7	18.6	-19.6	3.4	21.9	3.2	111	56	3.2	0.6	3.3 ± 0.2	5.3 ± 1.2	0.5
6937	UMa	4	18.6	-22.2	4.1	19.2	8.7	237	56	4.1	0.7	4.3 ± 0.3	16.0 ± 1.9	6.9
6983	UMa	6	18.6	-19.4	3.6	22.0	4.5	109	49	4.7	0.8	4.6 ± 0.3	3.6 ± 0.8	1.0
7095	UMa	4	18.6	-21.4	2.8	19.2	8.3	159	73	2.7	1.8	2.6 ± 0.1	13.1 ± 1.4	1.8
7323	dwarf	8	8.1	-18.9	2.2	21.2	2.7	86	47	3.0	0.4	2.9 ± 0.3	4.9 ± 1.5	0.4
7399	dwarf	8	8.4	-17.1	0.79	20.7	13.9	109	55	7.7	1.3	4.7 ± 0.5	21.3 ± 0.6	12.0
7524	dwarf	9	3.5	-18.1	2.6	22.2	3.1	79	46	7.2	0.3	6.9 ± 0.5	4.0 ± 0.8	0.2
7559	dwarf	10	3.2	-13.7	0.67	23.8	3.1	33	61	13.1	0.2	10.8 ± 5.2	4.3 ± 2.5	0.2
7577	dwarf	10	3.5	-15.6	0.84	22.5	2.7	18	63	0.9	0.4	0.7 ± 0.4	1.5 ± 1.5	0.3
7603	dwarf	7	6.8	-16.9	0.90	20.8	6.6	64	78	4.1	0.8	2.7 ± 0.5	9.2 ± 0.9	1.7
8490	dwarf	9	4.9	-17.3	0.66	20.5	16.2	78	50	4.4	0.4	3.3 ± 0.4	12.2 ± 0.5	1.2
8699	early	2	36.7	-20.7	3.7	22.2	6.5	183	73	12.0	0.8	8.2 ± 1.1	17.3 ± 2.5	1.1
9133	early	2	54.3	-22.6	9.1	21.3	11.2	229	53	10.0	1.0	8.1 ± 0.6	13.0 ± 1.3	1.6
9211	dwarf	10	12.6	-16.2	1.3	22.6	6.3	65	44	11.2	0.6	10.1 ± 1.8	6.2 ± 0.9	0.2
11670	early	0	12.7	-20.6	1.8	19.6	13.3	171	70	3.7	5.6	2.9 ± 0.2	37 ± 3	9.4
11707	dwarf	8	15.9	-18.6	4.3	23.1	3.5	100	68	9.3	0.8	9.4 ± 0.8	2.9 ± 0.4	2.0
11852	early	1	80.0	-21.5	4.5	20.7	20.6	165	50	8.5	0.3	7.6 ± 0.9	7.7 ± 0.8	0.4
12043	early	0	15.4	-18.6	0.84	19.9	19.6	94	67	2.6	10.2	1.9 ± 0.2	14.4 ± 0.4	6.6
12060	dwarf	10	15.7	-17.9	1.8	21.6	5.8	74	40	8.3	0.2	7.9 ± 0.8	3.2 ± 1.2	0.2
12632	dwarf	9	6.9	-17.1	2.6	23.5	3.3	76	46	15.1	1.1	14.1 ± 1.2	3.7 ± 0.9	1.3
12732	dwarf	9	13.2	-18.0	2.2	22.4	7.0	98	39	7.5	0.4	8.0 ± 0.6	5.7 ± 0.5	0.8

(1) UGC number, (2) source of the data; for the dwarf galaxies, the rotation curves and inclinations come from Swaters et al. (2009), distances and photometry from Swaters & Balcells (2002); for the Ursa Major cluster galaxies, all data come from Verheijen (1997), converted to the adopted cluster distance of 18.6 Mpc (Tully & Pierce 2000); for the early-type galaxies, data come from Noordermeer (2006) and Noordermeer et al. (2007), (3) numeric Hubble type, (4) adopted distance in Mpc, (5) absolute R -band magnitude, (6) R -band scale length in kpc, (7) extrapolated central R -band disc surface brightness, (8) radial extent of the rotation curve in units of scale lengths, (9) the rotation velocity at the last measured point in km s^{-1} , (10) inclination in degrees, (11, 12) maximum disc fit mass-to-light ratio, in units of M/L_{\odot} , and reduced χ^2 value for the fit (see Verheijen 1997; Noordermeer 2006; Swaters et al. 2011), (13,14,15) best-fitting values for the mass-to-light ratio, H I scale factor η , and reduced χ^2 value for the H I scaling model.

Hessman & Ziebart (2011) revisited this hypothesis, which they dubbed ‘the Bosma effect’, using a subset of 17 galaxies from The H I Nearby Galaxy Survey of de Blok et al. (2008). They concluded that the observed rotation curves could be explained nearly as well by scaling up the H I and stellar discs as by their models based on Burkert and NFW haloes.

The reason why the H I scaling appears to work and can repro-

duce the observed rotation curves is not clear. There have been various suggestions, including the presence of large amounts of cold gas in the disc (Pfenniger & Combes 1994), and hybrid models with both dark matter and cold gas (Revaz et al. 2009). It is important to emphasize here that the success of the H I scaling does not mean that all mass must reside in the baryonic disc, nor that dark matter haloes are unnecessary.

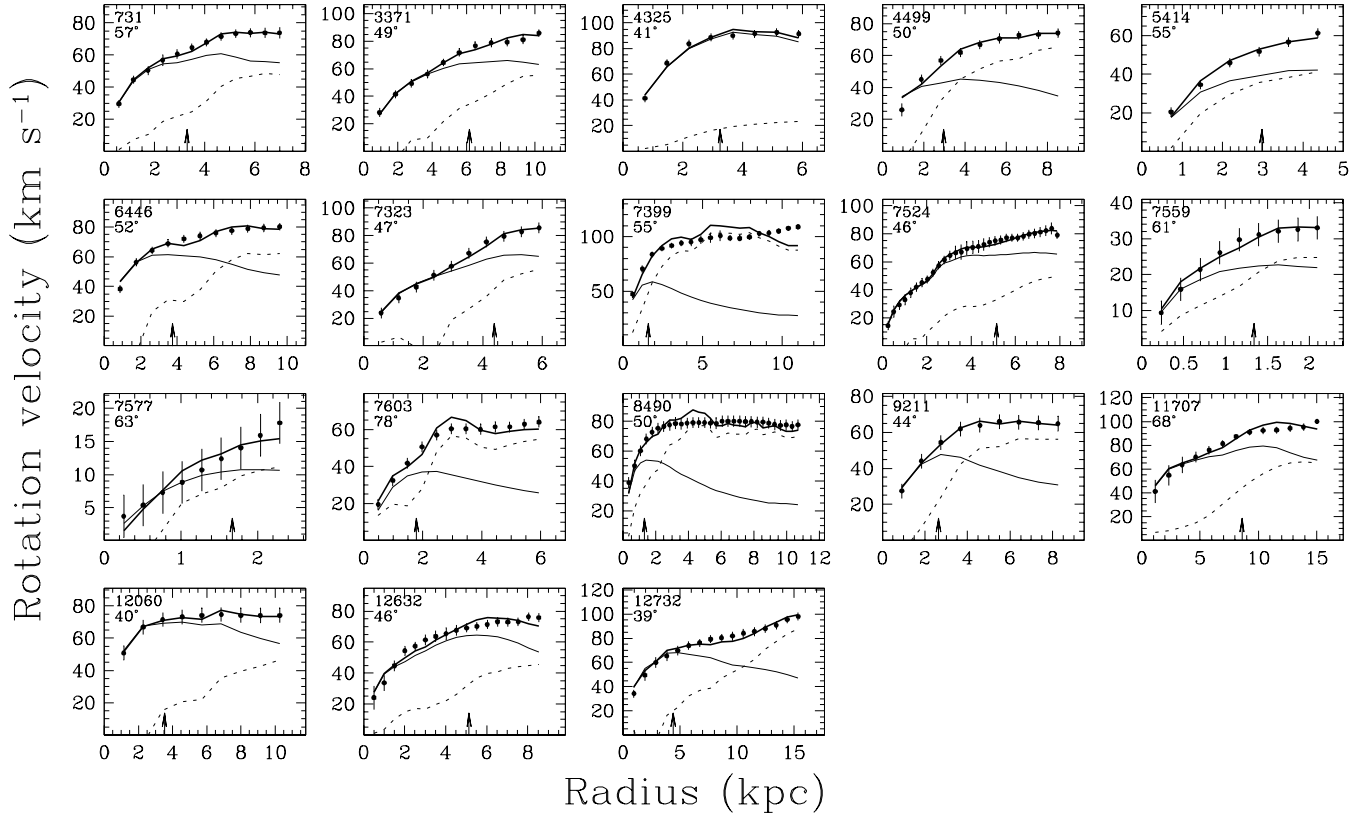


Figure 1. Mass models based on scaling the stellar disc and the H I component for the late-type dwarf galaxies in our sample. The filled circles represent the derived rotation curves. The thin full lines represent the contribution of the stellar discs to the rotation curves and the dotted lines that of the gas. The thick solid lines represent the best-fitting model based on scaling the contributions of the stars and the gas. The arrows at the bottom of each panel indicate a radius of two optical disc scale lengths. In the top left corner of each panel the UGC number and the inclination are given.

The purpose of the present article is to further explore how well the H I scaling works and to extend the study of HvAS to the larger sample of high-quality rotation curves that have recently become available for late-type dwarf galaxies (Swaters 1999; Swaters et al. 2009), early-type spiral galaxies (Noordermeer 2006), and late-type spiral galaxies in the Ursa Major cluster (Verheijen 1997; Verheijen & Sancisi 2001).

2 THE SAMPLE AND THE ROTATION CURVES

The sample presented here was selected from the dwarf galaxies presented in Swaters et al. (2009), from the Ursa Major sample from Verheijen (1997), which contains a large fraction of late-type spiral galaxies, and the early-type spiral galaxies presented in Noordermeer (2006).

The sample of late-type dwarf galaxies used here was observed as part of the WHISP project (Westerbork HI Survey of Spiral and Irregular Galaxies; see van der Hulst, van Albada & Sancisi (2001); Swaters et al. 2002). The galaxies in the WHISP sample were selected from the UGC catalogue (Nilson 1973), taking all galaxies with declinations north of 20° , blue major axis diameters larger than $1.5'$ and measured flux densities larger than 100 mJy. Selected from this list were the late-type dwarf galaxies, defined as galaxies with Hubble types later than Sd, supplemented with spiral galaxies of earlier Hubble types but with absolute B -band magnitudes fainter than -17 .

The galaxies in this sample have inclinations in the range $39^\circ \leq i < 80^\circ$. The lower limit of 39° was chosen to include UGC 12732 as well. Most of the galaxies in this sample have absolute magnitudes fainter than $M_R = -18$, as expected for dwarf galaxies. Only the 18 galaxies with the highest quality rotation curves as assigned by Swaters et al. (2009) were selected. The rotation curves were derived with a procedure that corrects for the effects of beam smearing to a large degree (Swaters et al. 2009). More details about this sample and its selection are provided in Swaters et al. (2011).

The late-type spiral galaxies in this sample used in this paper come from the H I study of galaxies in the Ursa Major cluster by Verheijen (1997; see also Verheijen & Sancisi 2001 and Verheijen 2001). This cluster is dominated by late-type spiral galaxies, but also contains galaxies with earlier and later types. The cluster is assumed to be at a distance of 18.6 Mpc (Tully & Pierce 2000).

We selected the galaxies from the sample presented in Verheijen (2001), which only includes galaxies with inclinations larger than 45° . In addition, we assigned a quality assessment to each rotation curve following Swaters et al. (2009), and only selected the 14 galaxies with the highest quality. The rotation curves in the Ursa Major sample have been corrected for the effects of beam smearing, through visual inspection and correction (see Verheijen & Sancisi 2001).

Finally, the early-type spiral galaxies come from the sample of Noordermeer (2006), also selected from the WHISP survey. For the selection of the early-type galaxies, however, a lower flux limit

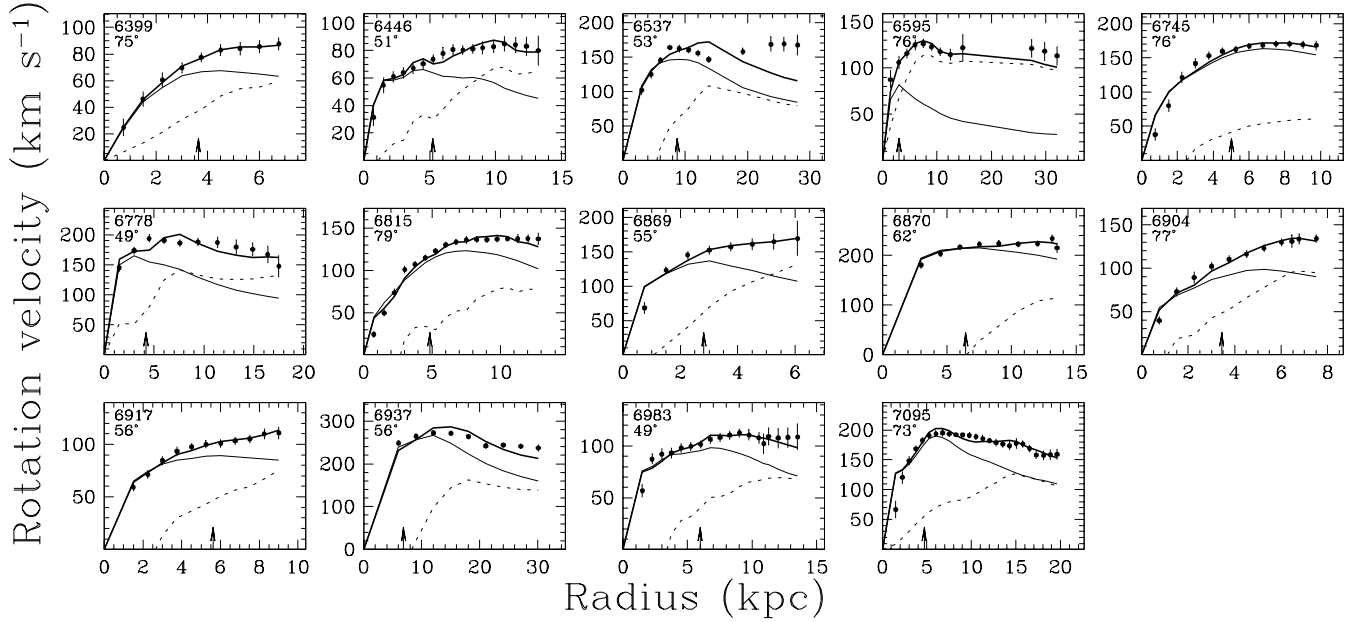


Figure 2. Same as Fig. 1 but for the galaxies in the Ursa Major sample.

of 20 mJy was used, made possible because of improvements to the Westerbork Synthesis Radio Telescope. More details about the sample selection can be found in Noordermeer et al. (2005).

The rotation curves for this sample are presented in Noordermeer et al. (2007). For this sample, the effects of beam smearing were mitigated by the use of high-resolution H α long-slit spectroscopic observations. For the study presented here, we only selected the 12 galaxies that have inclinations between 40° and 80° degrees, excluding the lowest quality rotation curves as given in Noordermeer et al. (2007).

We note that one galaxy, UGC 6446, is included in both the late-type dwarf and the Ursa Major sample. Because the data and the derived properties are completely independent, we have included both as an independent illustration of the uncertainties on the derived properties.

3 MASS MODELS

Assuming that a galaxy is axially symmetric and in equilibrium, its gravitational potential can be expressed as the sum of the individual mass components:

$$v_c^2 = v_*^2 + v_g^2 + v_h^2. \quad (1)$$

Here, v_c is the circular velocity, which is directly linked to the gravitational potential. The contribution of the stars to the rotation curve is given by v_* , v_g represents the contribution of the gas, and v_h that of the dark halo.

The contribution of the stars to the rotation curve consists of a bulge (usually not present in dwarf galaxies and late-type spiral galaxies) and the disc. Because we assume no prior knowledge of the stellar mass-to-light ratios, some value has to be assumed for both the bulge (Υ_b) and the disc (Υ_d). The contribution of the neutral H I gas to the rotation curve needs to be corrected for the contribution of helium and other elements. However, because in this paper we investigate how well the H I component can be scaled to explain the observed rotation curve, we use a free scale factor

η , omitting the dark halo term in Equation 1. Making this explicit, Equation 1 becomes:

$$v_{\text{rot}} = \sqrt{\Upsilon_b v_b^2 + \Upsilon_d v_d^2 + \eta v_{\text{HI}}^2}, \quad (2)$$

where v_b and v_d are the contribution of the bulge and stellar disc for a stellar mass-to-light ratio of unity, and v_{HI} is that of the H I only. This approach allows for dark matter as well, but it requires the rotation curve of dark matter is a linear combination of the rotation curves of the visible components.

The rotation curves have not been corrected for asymmetric drift. For the late-type dwarf galaxies, as was described in more detail in Swaters et al. (2009), the expected differences between the observed rotation velocity and the circular velocity are small (less than 1 km s⁻¹ in the inner parts of the rotation curves and less than 3 km s⁻¹ at all radii for 95% of the galaxies presented here). The spiral galaxies in our sample have higher rotation velocities, and asymmetric drift is expected to be less important there. A similar conclusion was reached by Dalcanton & Stilp (2010), who found that asymmetric drift is unlikely to be important for galaxies with rotation velocities over 75 km s⁻¹. We therefore used the observed rotation curves to represent the circular velocities.

In this paper, we only present mass models based on H I scaling. The maximum disc fit results presented in Table 1 are taken from Swaters et al. (2011), Verheijen (1997), and Noordermeer (2006) for the late-type dwarfs, late-type spirals, and early-type spirals, respectively.

3.1 The contribution of stars and gas

The contribution of the stellar disc to the rotation curve was calculated using the prescription given in Casertano (1983), using the R -band luminosity profiles presented in Swaters & Balcells (2002) for the late-type dwarf galaxies, the K -band profiles presented in Tully et al. (1996) for the galaxies in the Ursa Major sample, and the R -band profiles from Noordermeer & van der Hulst (2007) for the early-type spiral galaxies.

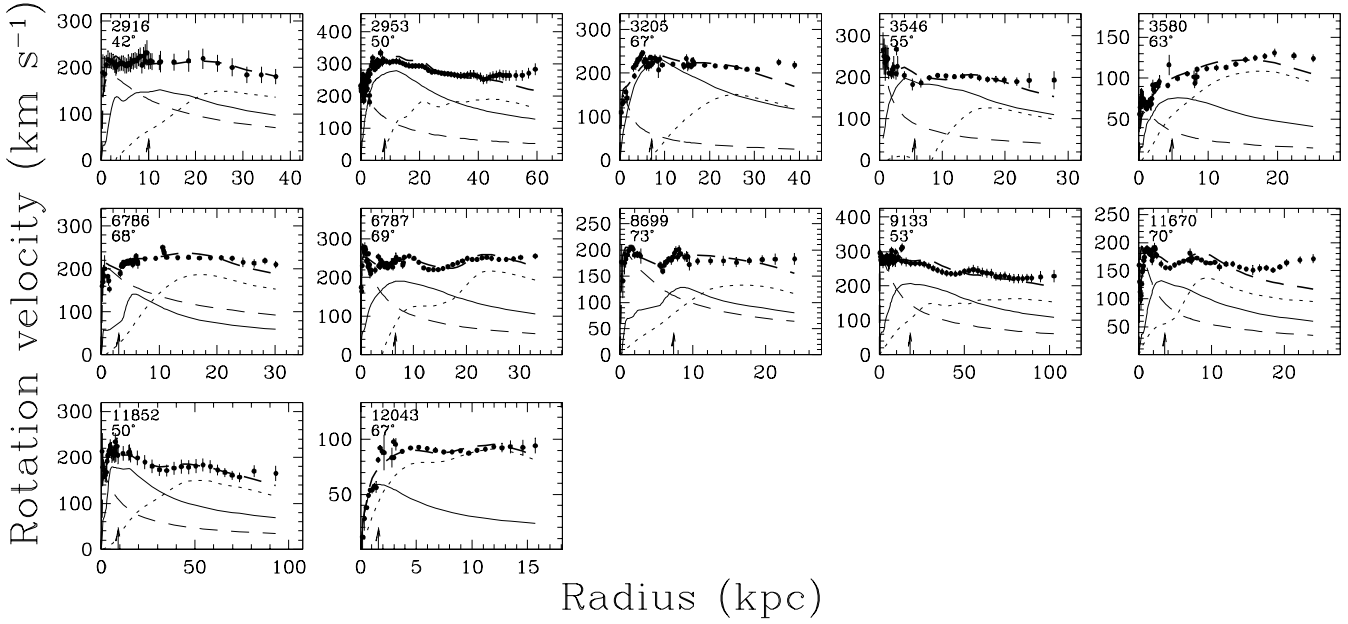


Figure 3. Same as Fig. 1 but for the early-type galaxies. The long-dashed line represents the contribution of the stellar bulge.

The contribution of the HI was also calculated using the prescription from Casertano (1983), using the HI radial profiles from Swaters et al. (2002), Verheijen & Sancisi (2001), and Noordermeer et al. (2005).

For the mass models presented here we have used the same assumptions for the disc and bulge parameters as the original papers. This means that there are small differences in the adopted thicknesses and vertical density profiles. For example, both Noordermeer (2006) and Swaters et al. (2011) adopted an exponential vertical distribution with a scale height one fifth of the scale length. Verheijen (1997), on the other hand, adopted a vertical sech^2 distribution, but with the same relative scale height. For the HI disc, both Swaters et al. (2011) and Noordermeer (2006) assume the same vertical distribution for the HI as for the stellar disc, whereas Verheijen (1997) adopted an infinitely thin HI disc. However, these differences are of little consequence for the study presented here. Not only are the effects of these different assumptions less than a few percent (Swaters 1999; Noordermeer 2006; Swaters et al. 2011), but the effects are most important in the inner regions. Thus, the assumptions will have no significant effect on the derived HI scale factor η .

For the bulge contribution, we used the same decomposition as presented in Noordermeer (2006). Following Verheijen (1997), no bulge-disc decomposition was used for the galaxies in the Ursa Major sample, because most of the galaxies have weak or no bulges.

We assumed that the disc mass-to-light ratio Υ_{d}^R and the bulge mass-to-light ratio Υ_{b}^R are independent of radius.

3.2 Rotation curve fits

The relative contribution of each of the different mass components is determined by a simultaneous fit of the right-hand side of Eq. 2 to the observed rotation curve. For dwarf and late-type spiral galaxies, which have no or no significant bulge, this means there are only two free parameters, Υ_{d}^R and η . For the early-type galaxies, Υ_{b}^R is the third free parameter.

All the fits to rotation curves are shown in Figs. 1, 2, and 3.

The fit parameters are listed in Table 1. The uncertainties on the fitted parameters have been derived from the 68% confidence levels and include the covariance between Υ_{d}^R and η . The uncertainties on the derived rotation velocities are non-Gaussian, as the points in the rotation curves are correlated, and the rotation curves and their uncertainties can be affected by systematic effects. The confidence levels and the corresponding uncertainties should be considered estimates.

The bulge mass-to-light ratios Υ_{b}^R are not given in Table 1 because they are not used in this paper. However, they are presented in Noordermeer (2006). The fits for the Ursa Major galaxies where done with K -band light profiles presented in Tully et al. (1996). For ease of comparison to the late-type dwarf and early-type spiral galaxies, the K -band mass-to-light ratios were converted to the R -band.

4 RESULTS

As can be seen from Figures 1, 2, and 3, for the majority of the galaxies in our sample good fits to the rotation curves can be obtained solely by scaling the contributions of the stellar and HI discs. This is remarkable given that there are only two free parameters in most of these fits, and three free parameters for the early-type galaxies with bulges. Even with only two or three free parameters, the HI scaling model can explain rising rotation curves such as seen in UGC 12732 (see Figure 1), and declining rotation curves such as seen in UGC 7095 (see Figure 2). In some cases, it can even explain large-scale features in the rotation curves, such as UGC 6787 and UGC 11852 (see Figure 3).

Although the model is successful at explaining the rotation curves of the vast majority of the galaxies in our sample, there are some problem cases. For the late-type dwarf galaxies (Figure 1), there is a clear discrepancy between the model and the observed rotation curve for only one of the galaxies, UGC 7399. We note that this galaxy has a lopsided appearance in HI, with the HI extending almost twice further on one side of the galaxy than on the other.

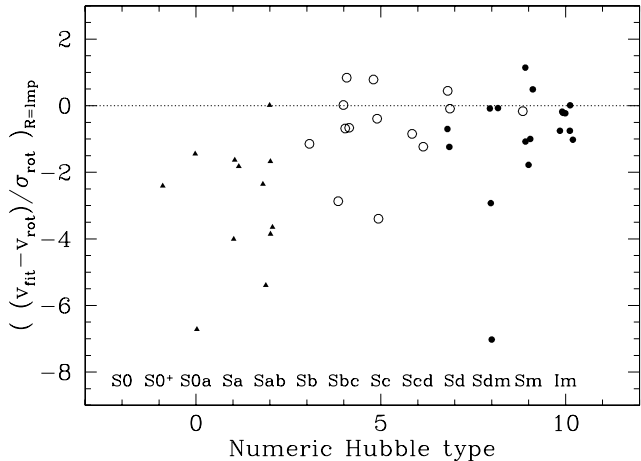


Figure 4. The difference between the fitted model and the observed rotation curve at the last measured point of the rotation curve, divided by the uncertainty on the rotation velocity. Triangles represent data from Noordermeer et al. (2007), circles represent data from Verheijen (2001), and dots represent data from Swaters et al. (2011). A random value between -0.4 and 0.4 has been added to the numeric Hubble type to spread the points in the plot.

Because of this strong deviation from axisymmetry, the derived H I profile is likely not to be representative of the true radial H I distribution. In two other galaxies, UGC 7603 and UGC 8490, the model does predict the overall shape correctly, but there are some wiggles in the model that are not seen in the observed rotation curve.

For the late-type spiral galaxies (Figure 2), there is also only one galaxy for which H I scaling clearly cannot explain the observed rotation curve, UGC 6537. This galaxy has the strongest warp in the Ursa Major sample, and for the most discrepant points in the fit, the rotation curve has only been derived from one side.

For the early-type spiral galaxies (Figure 3), the H I scaling does not appear to work as well as for the late-type dwarf and late-type spiral galaxies. As was also noted by Noordermeer (2006), the H I scaling tends to give poorer results in the outer regions (see e.g., UGC 2953, UGC 3205, UGC 3580, and UGC 11670).

How well H I scaling can explain the observed rotation curve at large radii is shown in Figure 4, where the difference between the model and the observed rotation velocity, divided by the uncertainty in the rotation velocity, at the last measured point of the rotation curve is plotted against the numeric Hubble type. Whereas for late-type spiral and dwarf galaxies the model is close to observed rotation curve (with the exception of UGC 7399 as explained above), for early-type spiral galaxies the last measured point is on average 3σ above the model.

Interestingly, except perhaps for UGC 11670 and UGC 2953, the discrepancy between our model and the observed rotation curves is seen only in the data points derived from the velocity fields convolved to $60''$. Although such a convolution is needed to reach the lowest H I column densities, the additional convolution will also exacerbate the effects of beam smearing, especially at higher inclinations. Indeed, for the seven galaxies with inclinations near 70° , the model falls on average 4σ below the model, for the four galaxies with inclinations near 50° the difference is 2σ on average, and for the one galaxy near 40° the model is in agreement with the observed rotation curve. Although the relatively small number of galaxies precludes a clear conclusion, such a dependence on inclination is not expected if the model itself were

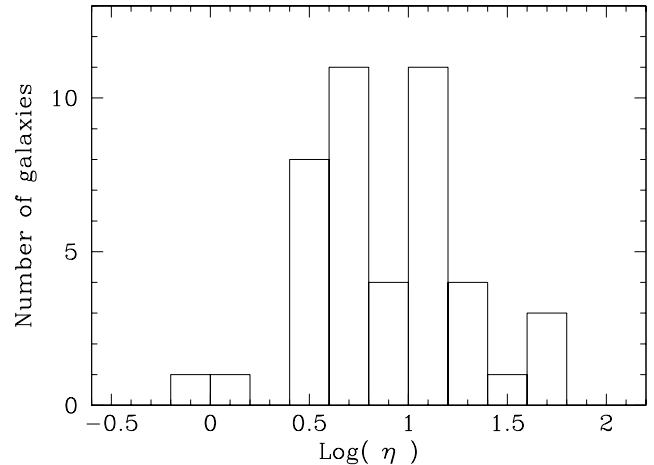


Figure 5. Distribution of the best-fitting H I scaling factors η .

incorrect. We will discuss the early-type galaxies further in Section 5.

4.1 H I scale factors

Over our entire sample, the log-average scale factor is 8.2, similar to the log-average of 10.2 found by HvAS. However, as can be seen in Figure 5, there is a considerable range in the scale factors, ranging from near unity for two of the late-type dwarf galaxies, to around fifty for some of the early-type spiral galaxies.

As can be seen in Figures 6, 7, and 8, the scale factor η is correlated with numeric Hubble type, central disc surface brightness, and absolute magnitude, respectively. Galaxies with later Hubble types, fainter surface brightnesses, and fainter absolute magnitudes tend to have lower scale factors. Galaxies with a numeric Hubble type of 5 or later have a log-average scale factor of ~ 5 , whereas galaxies with earlier Hubble types have a log-average η of ~ 16 . Although not shown here, η is also correlated with the maximum rotation velocity, as was already noted by Bosma (1978).

Interestingly, η is also correlated with the extent of the rotation curve, when expressed in units of disc scale lengths, as can be seen in Figure 9. Several factors, each discussed below, likely play a role here, including the ratio of optical to H I scale lengths, the details of the fitting process, and intrinsic correlations.

As was pointed out by HvAS, the extent of the rotation curve when expressed in units of the H I disc scale length (assuming that the H I distribution is roughly exponential) is relatively constant. Ignoring possible central depressions, the central H I surface density is relatively constant among galaxies (about $7 M_\odot \text{pc}^{-2}$ for the galaxies in our sample with a dispersion of $3 M_\odot \text{pc}^{-2}$). For the late-type spiral and dwarf galaxies in our sample, the rotation curves could be derived out to an H I surface density of about $1 M_\odot \text{pc}^{-2}$, corresponding to about 2 H I scale lengths. For the early type galaxies, the H I observations are more sensitive, and the rotation curve could typically be determined out to an H I surface density of about $0.25 M_\odot \text{pc}^{-2}$, corresponding to about three H I scale lengths.

This relatively constant extent of the rotation curves of roughly 2-3 H I scale lengths means that if a rotation curve has a large ratio of r_{max}/h , the H I is more extended relative to the optical disc, and hence the rotation curve of the H I only peaks farther outside the optical disc. The more extended the H I is relative to the

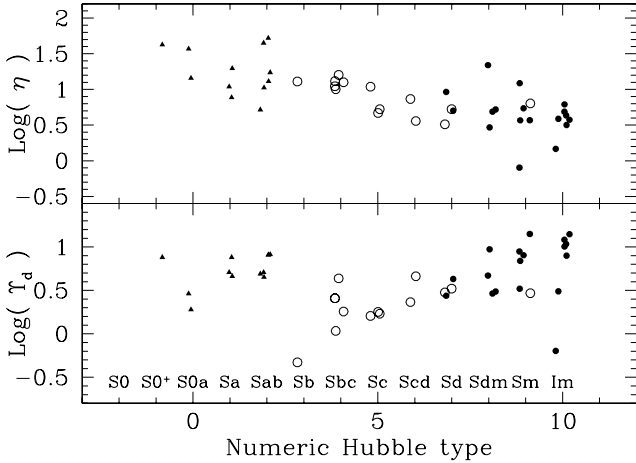


Figure 6. H I scaling factors η (top panel) and Υ_d^R (bottom panel) vs. numerical Hubble type. Symbol coding as in Figure 4.

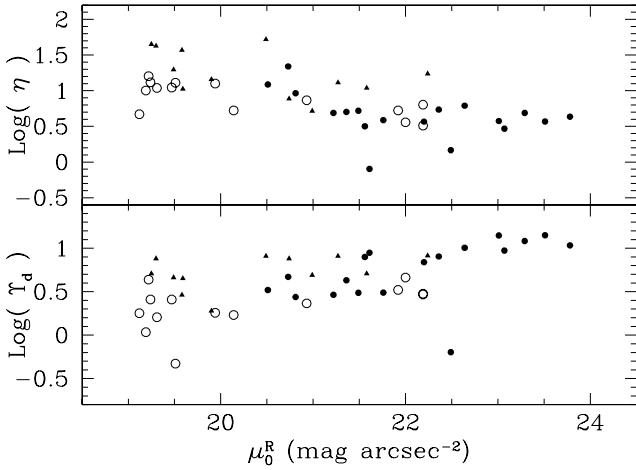


Figure 7. H I scaling factors η (top panel) and Υ_d^R (bottom panel) vs. R -band extrapolated central disc surface brightness. Symbol coding as in Figure 4.

optical, the less the optical contributes at the radius where the H I peaks, and thus the H I needs to be scaled up more to explain the observed rotation curve.

Similarly, for early type galaxies, the presence of a maximum bulge tends to depress the contribution of the stellar disc in the fits, and thereby increases the scaling of the H I component further. Also, if the contribution of the stellar disc in the fits is not maximal (as appears to be the case for UGC 7399 and UGC 8490 in Figure 1, this also will result in a higher value for η in the fits.

Distance uncertainties can also affect the scale factors, but, given the generally large distances to the early type galaxies, this will not change the scale factors significantly.

However, all these effects are relatively small, and cannot explain the high scale factors of up to 50 seen among some of the early type galaxies. Thus, it appears likely that some of the variation in scale factors between galaxies is real.

4.2 Stellar mass-to-light ratios

As can be seen in Figure 10, the stellar mass-to-light ratios found in our models are similar to those found in the maximum disc fits

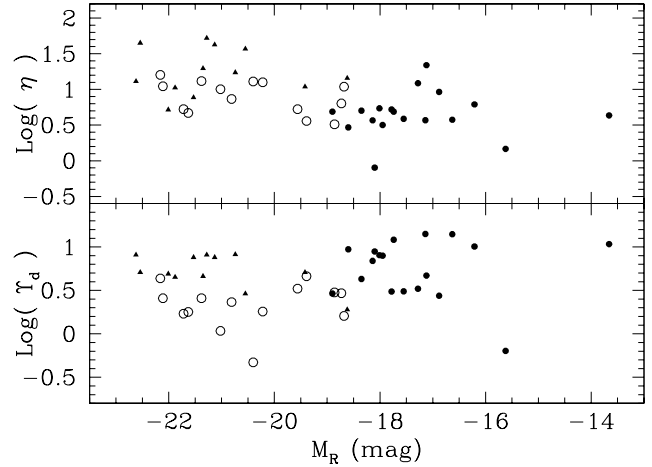


Figure 8. H I scaling factors η (top panel) and Υ_d^R (bottom panel) vs. absolute R -band magnitude. Symbol coding as in Figure 4.

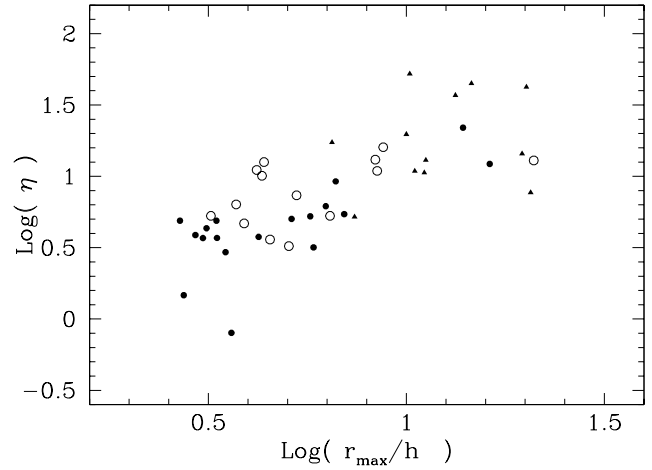


Figure 9. H I scaling factors η vs. maximum radial extent of the rotation curves in units of optical disc scale lengths. Symbol coding as in Figure 4.

(see e.g., Verheijen 1997; Noordermeer 2006; Swaters et al. 2011). The values for Υ_d^R range from 0.5 up to around 15. The high end of this range is well outside of the range predicted by current stellar population synthesis models (e.g., Bell et al. 2003; Zibetti, Charlot & Rix 2009).

We explored the correlation of Υ_d^R with other global properties. Because Υ_d^R is similar to those of maximum disc models (see Figure 10), these correlations are similar to those found for the maximum disc models. We find that Υ_d^R is weakly correlated with surface brightness (see Figure 7; see also Swaters et al. 2011), but Υ_d^R is not clearly correlated with Hubble type or absolute magnitude (see Figures 6 and 8, respectively). In addition, as shown in Figure 11, Υ_d^R is not correlated with η , indicating that the two scale factors are independent of each other.

Although not shown in Table 1, we have also determined Υ_b^R , the mass-to-light ratio for the bulge for the maximum disc and H I scaling fits. Here too we find that Υ_b^R is similar between the two fits, although Υ_b^R is approximately 10% larger in the H I scaling fits.

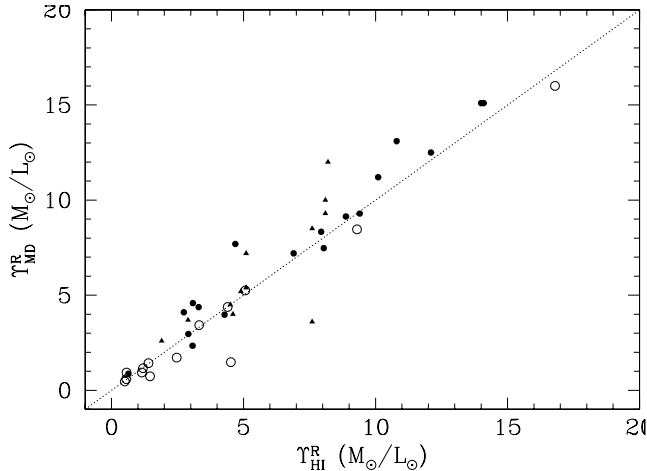


Figure 10. Comparison of the R-band mass-to-light ratios for the HI scaling models and those found in the maximum-disc fits. Symbol coding as in Figure 4. The dotted line is the line of equality.

5 DISCUSSION

5.1 Baryons distribution vs. rotation curve shape

Previous studies have already shown that in almost all galaxies the rotation curves of the stellar discs can be scaled up to explain all of the observed rotation curves out to two or three disc scale lengths in spiral galaxies (e.g. Kalnajs 1983; Kent 1986; Palunas & Williams 2000) and in dwarf and LSB galaxies (e.g., Swaters, Madore & Trewheella 2000; Swaters et al. 2011). Thus, the detailed distribution of the light appears to be linked to the rotation curve shape. This link suggests a coupling between the distributions of the total mass and the stellar mass. (Sancisi 2004; Swaters et al. 2009).

In this paper we have shown that for the vast majority of the rotation curves of the 43 disc galaxies in our sample, ranging from early-type spirals to late-type dwarf galaxies, the observed rotation curves can be explained by combining and scaling the contributions of both the stars and the H I to the rotation curves. This is consistent with the results found previously by Bosma (1981) and confirms and extends those of HvAS.

The link between the rotation curve shape and the galactic discs is therefore not limited to the stars, but appears to extend to the H I discs as well. The molecular gas tends to follow the distribution of the stars (e.g., Regan et al. 2001), so its contribution is effectively included in that of the stars in our fits. Therefore, the link between the rotation curve shape and the galactic discs seems to extend to all the baryons in the disc. We refer to this as the ‘baryonic scaling model’, because the observed rotation curves can be explained by scaling both tracers of the baryonic mass.

The baryonic scaling model requires two free parameters, namely the scale factors of the stellar and H I discs (fits to galaxies with bulges have three free parameters). Whereas for mass models including dark halos there is usually a large range in acceptable fits (e.g., van Albada et al. 1985; Dutton et al. 2005; Swaters et al. 2011), for the baryonic scaling models there is only a small range over which acceptable fits can be found. For the baryonic scaling, there is no degeneracy in the fits because the contributions of gas and stars to the rotation curve peak at different radii and hence are independent (except in a few cases, such as UGC 4325 and UGC 5414). Moreover, for baryonic scaling to work, as was shown

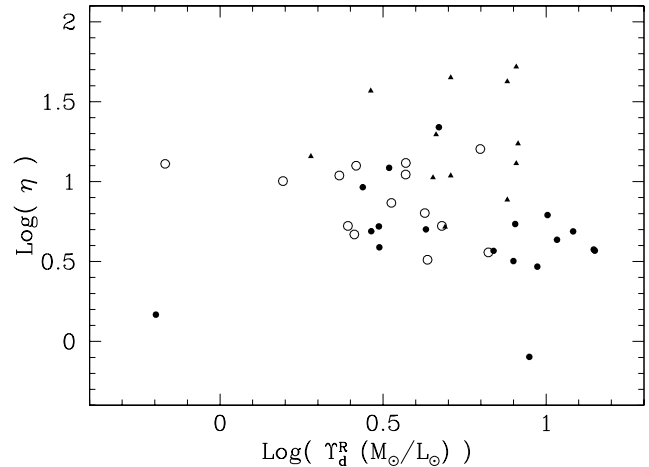


Figure 11. H I scaling factors η vs. Υ_{d}^R . Symbol coding as in Figure 4.

in Section 4.2, and as was also found by HvAS and Hessman & Ziebart (2011), a (near-)maximal disk is required.

Despite this limited freedom in the fits, the baryonic scaling can explain the observed breadth of rotation curve shapes, from early-type spiral galaxies with steeply rising inner rotation curves and declining outer parts, to those of late-type dwarf galaxies with rotation curves that rise more slowly. Even more remarkably, baryonic scaling can also explain large-scale features in some of the observed rotation curves (see e.g., Figure 3; Broeils 1992b). We must caution, however, that features in the rotation curves may have different origins, such as streaming motions along spiral arms. A one-to-one correlation between features in the observed rotation curve and the H I distribution is therefore not expected.

A global link between the baryons in a galaxy and its rotation velocity has already been established in the baryonic Tully-Fisher relation (e.g., McGaugh et al. 2000). However, this baryonic Tully-Fisher only links the observed baryonic mass to the amplitude of the rotation curve. The fact that the baryonic scaling model works well indicates that at a more local level there is also a link between the distributions of the baryons and the rotation curve shape. Because the rotation curve reflects the total mass distribution, the success of the baryonic scaling model suggests a relation exists between the distribution of the total mass and the distribution of the baryons.

5.2 The H I scale factor

HvAS used a simple relation to estimate the H I scale factor, assuming that the mass distribution in a galaxy can be described by two exponential discs, one for the stars and one for the H I. Using this, HvAS derived that the scale factor η can be written as:

$$\eta = \frac{\Sigma_{\text{stars},0} h_{\text{stars}}}{\Sigma_{\text{gas},0} h_{\text{gas}}}, \quad (3)$$

where $\Sigma_{\text{stars},0}$ and $\Sigma_{\text{gas},0}$ are the central surface mass densities of the stars and the gas, and h_{stars} and h_{gas} the exponential scale lengths of the stars and the gas. The ratio of the scale lengths of the stellar and H I discs is roughly constant (to about a factor of two for the sample presented here). The H I central surface mass $\Sigma_{\text{gas},0}$ varies by a similar amount (e.g., Swaters et al. 2002). However, $\Sigma_{\text{stars},0}$ varies by a factor of 40 across our sample, and is much higher for high surface brightness galaxies. Thus, the scale factor

η is expected to vary with surface brightness, as is seen in Figure 7. Because later-type galaxies, and galaxies with fainter absolute magnitudes are more likely to have lower surface brightnesses, the trend seen with surface brightness may also explain the trends of η with Hubble type and absolute magnitude.

5.3 Baryonic scaling works

This study clearly shows that the HI scaling previously discussed by HvAS for a smaller sample, works well: regardless of whether the stellar and HI discs are near maximal or significantly sub-maximal, the total mass density distribution inferred from rotation curves can be reproduced by scaling the density distributions of the stars and the HI. This relation between the distribution of both the stars and the HI on the one hand, and the distribution of the total mass on the other seems to extend the idea of a coupling between the distribution of light and total mass as found previously (e.g., Sancisi 2004; Swaters et al. 2009) to all baryons in the disc.

The success of the baryonic scaling model may be readily understood if the baryons are the dominant mass component. Indeed, in the baryonic scaling model, the stellar disc must be maximal to explain the inner parts of the rotation curves (see Figure 10). However, observational evidence appears to indicate that discs tend to be submaximal (e.g., Bottema 1997; Courteau & Rix 1999; Swaters 1999; Kregel, van der Kruit & de Grijs 2002; Kranz, Slyz & Rix 2003; Ciardullo et al. 2004; Herrmann et al. 2009; Westfall et al. 2011; Bershadsky et al. 2011). As was also pointed out by Hessman & Ziebart (2011), the stellar light distribution can also be considered as a proxy for the molecular gas. The maximal discs found in our baryonic scaling model may therefore not represent maximal stellar discs, but rather reflect the combination of the stellar disc and a molecular gas component. Still, adding the estimated molecular gas masses to the stellar disc masses cannot explain the high values for Υ_d^R seen in some of our fits. Therefore, if the baryons were the dominant mass component, an additional cold gas component would be needed.

Several ideas have been put forward for such a cold gas component, considering both the observed rotation curves and arguments of disc stability (e.g., Pfenniger & Combes 1994; Revaz et al. 2009). The latter authors propose the presence of a 'dark gas' with a velocity dispersion much larger than that of the HI. Additional indications that there is more mass in the outer HI discs than the HI alone are e.g. the existence of spiral structure in extended HI discs (e.g., NGC 2915; Masset & Bureau 2003) and the kinematics of the polar ring galaxy NGC 4650A (Combes & Arnaboldi 1997).

In this paper we have used two independent scale factors for the contributions of the stars and gas to the observed rotation curve. It is tempting to speculate whether a single scale factor could link the combined contribution of the baryons to the observed rotation curve. The scale factors Υ_d^R and η have an average range of around ten to twenty (see Figures 6, 7, and 8). This range is too large to be explained by variations in the stellar mass-to-light ratios or by the contribution of molecular gas. To bring the scale factors together one has to assume the presence of a dark baryonic component that follows the gas distribution.

Alternatively, the success of the baryonic scaling model may imply a coupling between the distribution of the baryons and that of the dark matter. For example, HvAS tested the hypothesis that the dark matter density is a scaled version of the HI density, and others have interpreted the success of the HI scaling in the same way (e.g., Meurer & Zheng 2011). This coupling is only straightforward to

understand if the dark matter is in the disc or in a highly flattened halo. If the dark matter halo has a spherical shape, however, the radial distribution of the dark matter will be different from that of the stars and gas for the same rotation curve shape.

We have also explored baryonic scaling in the context of MOND (Milgrom 1983a,b). We created a set of MOND models by assuming an exponential stellar disc, and using the average HI profile from Swaters et al. (2002). With this as input, we calculated the expected MOND rotation curves for a range of different disk surface brightnesses, assuming the acceleration parameter $a_0 = 1.0 \times 10^{-8} \text{ cm s}^{-2}$. We then fit our baryonic scaling model to these model MOND rotation curves. The fits are generally good, and result in HI scale factors between ~ 6 and ~ 10 , with lower values found at lower surface brightnesses. The baryonic scaling model therefore is consistent with MOND.

Finally, it is possible that the success of the baryonic scaling model could at least in part be due to the fact that the different baryonic components all peak at different radii, which means their individual rotation curves can be combined to create a roughly flat rotation curve.

5.4 Baryonic scaling in early-type spiral galaxies

Whether or not HI scaling works by virtue of the HI and stellar rotation curves peaking at different radii can in principle be tested by studying galaxies for which the rotation curves extend past the peak in the HI rotation curves. The early-type galaxies in our sample make this possible, because for these galaxies the rotation curves extend to lower HI column densities (see Section 4.1 and Figure 3). At first sight, as shown in Figure 4, the results may indicate that the HI scaling model starts to fail for these more extended galaxies, because for all but one of these galaxies, the model falls below the observed rotation curve.

However, there are several factors that may contribute to this difference. For example, some of the HI flux may be missing, either due to the intrinsic limitations of an interferometer, or due to the method of deriving integrated HI maps, which usually includes a thresholding step to select areas with emission. Also, it is possible that at the low column densities observed at large radii the HI starts to become ionized, e.g., due to intergalactic ionizing background radiation (e.g., Bochkarev & Sunyaev 1977) or ionizing radiation from the bright disk (e.g., Bland-Hawthorn & Maloney 1999) in case of warps. Thirdly, it is possible that the kinematics of the outermost regions do not follow the kinematics of the inner regions, e.g., due to warps, outer spiral arms, or interactions. Finally, as noted in Section 4, the outermost points for rotation curves of the early-type galaxies were derived from lower-resolution data, so it is possible that beam smearing affected the derived rotation velocities, especially for galaxies at higher inclinations.

6 SUMMARY AND CONCLUSIONS

We have presented mass models for a sample of 43 disc galaxies, ranging from early-type spiral to late-type dwarf galaxies, that are based on scaling up the stellar and HI discs. Our baryonic scaling models fit the observed rotation curves well in the vast majority of cases, even though the models have only two or three free parameters, namely the scale factors, while the shapes of the rotation of the stars and the gas are fixed. These models also reproduce some of the detailed large-scale features of rotation curves. In particular for early-type spiral galaxies the models sometimes fail at

large radii. This may signal a real problem for the model, but it can also be caused by observational effects, the analysis methods used, or ionization of the H I at low column densities. The average H I scale factor η we find is around 8 (or 6 after correcting for the contribution of primordial helium), although η can vary considerably from galaxy to galaxy. The scale factor depends on galaxy properties, and decreases towards lower surface brightnesses, later Hubble types, and fainter absolute magnitudes. These results confirm and extend those of HvAS.

A global link between the baryonic mass of a galaxy and the amplitude of its rotation curve has already been established in the baryonic Tully-Fisher relation. The success of the baryonic scaling model indicates there is a more local coupling between the distribution of the baryons and the rotation curve *shape*. Because the observed rotation curve is a reflection of the distribution of the total mass, the success of the baryonic scaling model suggests a relation between the distributions of the baryons and that of the total mass.

REFERENCES

- Begeman K. 1987, PhD thesis, Rijksuniversiteit Groningen (<http://irs.ub.rug.nl/ppn/291578543>)
- Bell E.F., Baugh C.M., Cole S., Frenk C.S., Lacey C.G., 2003, MNRAS 343, 367
- Bershady M. A., Martinsson T. P. .K, Verheijen M. A. W., Westfall K. B., Andersen D. R., Swaters R. A., 2011, ApJ, 739, L47
- Bland-Hawthorn, J., Maloney, P. R., 1999, ApJ, 510, L33
- Bochkarev, N. G., Sunyaev, R. A., 1977, Soviet Astron., 21, 542
- Bosma A., 1978, PhD thesis, Rijksuniversiteit Groningen
- Bosma A., 1981, AJ, 86, 1825
- Bottema R. 1997, A&A, 328, 517
- Broeils A.H., 1992a, PhD thesis, Rijksuniversiteit Groningen
- Broeils A.H., 1992b, A&A 256, 19
- Carignan C., 1985, ApJ 299, 59
- Carignan C., Puche, D., 1990, AJ, 100, 641
- Casertano S. 1983, MNRAS 203, 735
- Ciardullo R., Durrell P. R., Laychak M. B., Herrmann K. A., Moody K., Jacoby G. H., Feldmeier J. J., 2004, ApJ, 614, 167
- Combes F., Arnaboldi M., 1996, A&A, 305, 763
- Courteau S., Rix H.-W., 1999, ApJ, 513, 561
- Dalcanton J. J., Stilp A. M., 2010, ApJ, 721, 547
- de Blok W. J. G., Walter F., Brinks E., Trachternach C., Oh S.-H., Kennicutt R. C., Jr., 2008, AJ, 136, 2648
- Dutton A. A., Courteau S., de Jong R., Carignan C., 2005, ApJ, 619, 218
- Herrmann K. A., Ciardullo R., 2009, ApJ, 705, 1686
- Hessman F. V., Ziebart M., 2011, A&A, 532, A121
- Hoekstra H., van Albada T. S., Sancisi R., 2001, MNRAS, 323, 453 (HvAS)
- Jobin M., Carignan C., 1990, AJ 100, 648
- Kalnajs A.J., 1983, in Athanassoula E., ed, IAU Symp. 100, Internal Kinematics of Galaxies, p. 87
- Kent S.M., 1986, AJ 91, 1301
- Kranz T., Slyz A., Rix H.-W., 2003, ApJ, 586, 143
- Kregel M., van der Kruit P. C., de Grijs R., 2002, MNRAS, 334, 646
- Masset F. S., Bureau M., 2003, ApJ, 586, 152
- McGaugh S. S., Schombert J. M., Bothun G. D., de Blok W. J. G., 2000, ApJ, 533, L99
- Meurer G. R., Zheng Z., 2011, BAAS, 43, #246.13
- Milgrom M., 1983a, ApJ, 270, 365
- Milgrom M., 1983b, ApJ, 270, 371
- Nilson P., 1973, Uppsala General Catalogue of Galaxies, Uppsala Astr. Obs. Ann., Vol. 6
- Noordermeer E., 2006, PhD thesis, Rijksuniversiteit Groningen (<http://irs.ub.rug.nl/ppn/292030207>)
- Noordermeer E., van der Hulst J. M., 2007, MNRAS, 376, 1480
- Noordermeer E., van der Hulst J. M., Sancisi R., Swaters R. A., van Albada T. S., 2005, A&A, 442, 137
- Noordermeer E., van der Hulst J. M., Sancisi R., Swaters R. S., van Albada T. S., 2007, MNRAS, 376, 1513
- Palunas P., Williams T. B., 2000, AJ, 120, 2884
- Pfenniger D., Combes F., 1994, A&A, 285, 94
- Regan M. W., Thornley M. D., Helfer T. T., Sheth K., Wong T., Vogel S. N., Blitz L., Bock D. C.-J., 2001, ApJ, 561, 218
- Revaz Y., Pfenniger D., Combes F., Bournaud F., 2009, A&A, 501, 171
- Sancisi, R., 2004, IAU Symp. 220, ASP Conf series, p. 223
- Swaters R.A., 1999, PhD thesis, Rijksuniversiteit Groningen (<http://irs.ub.rug.nl/ppn/186373880>)
- Swaters R. A., Balcells M., 2002, A&A, 390, 863
- Swaters R. A., Madore B. F., Trewhella M., 2000, ApJ, 531, L107
- Swaters R.A., Sancisi R., van Albada T. S., van der Hulst J. M., 2009 A&A 493, 871
- Swaters R. A., Sancisi R., van Albada T. S., van der Hulst J. M., 2011, ApJ, 729, 118
- Swaters R.A., van Albada T. S., van der Hulst J. M., Sancisi R., 2002 A&A 390, 829
- Tully R. B., Pierce M. J., 2000, ApJ, 533, 744
- Tully R. B., Verheijen M. A. W., Pierce M. J., Huang J.-S., Wainscoat R. J., 1996, AJ, 112, 2471
- van Albada T.S., Bahcall J.N., Begeman K., Sancisi R., 1985, ApJ 295, 305
- van der Hulst J. M., van Albada T. S., Sancisi R., 2001, Gas and Galaxy Evolution, 240, 451
- Verheijen M.A.W., 1997, PhD thesis, Rijksuniversiteit Groningen (<http://irs.ub.rug.nl/ppn/163958270>)
- Verheijen M. A. W. 2001, ApJ, 563, 694
- Verheijen M. A. W., & Sancisi R., 2001, A&A, 370, 765
- Westfall K. B., Bershady M. A., Verheijen M. A. W., Andersen D. R., Martinsson T. P. .K, Swaters R. A., Schechtman-Rook A., 2011, ApJ, 742, 18
- Zibetti S., Charlot S., Rix H.-W., 2009, MNRAS 400, 1181